INCLUSIVE CHARGED AND NEUTRAL PARTICLE PRODUCTION AND SEARCH FOR RELATIVISTIC PARTICLES WITH FRACTIONAL ELECTRIC CHARGE AT THE CERN $p\bar{p}$ COLLIDER

The UA2 Collaboration*)
(Univ. Bern, CERN, NBI Copenhagen,
LAL Orsay, Univ. and INFN Pavia, CEN Saclay)

Presented by: C. Conta
INFN and University of Pavia, Italy

Abstract - We present results on the production of charge and neutral particles at large angle at an energy $\sqrt{s}$ = 540 GeV. No evidence has been found for the existence of light relativistic quarks.

*Members of the UA2 Collaboration:
M. Banner, Ph. Bloch, F. Bonaudi, K. Borer, M. Borghini, J.-C. Chollet, A.G. Clark, C. Conta, P. Darriulat, L. Di Lella, J. Dines-Hansen, P.-A. Dorsaz, L. Fayard, M. Fraternali, D. Foideveaux, J.-M. Gaillard, D. Gildemeister, V.G. Goggi, H. Grote, B. Hahn, H. Hanni, J.R. Hansen, P. Hansen, T. Himel, V. Hungerbuhler, P. Jenni, O. Kofoed-Hansen, M. Livan, S. Loucatos, B. Madsen, P. Mani, B. Mansoulié, G.C. Mantovani, L. Mapelli, B. Merkel, M. Mermikides, R. Mollerud, B. Nilsson, C. Onions, G. Parrour, F. Pastore, H. Plothow-Besch, N. Prevot, J.-P. Repellin, A. Rothernberg, A. Roussarie, G. Sauvage, J. Schacher, J.L. Siegrist, F. Stocker, J. Teiger, V. Vercesi, H.H. Williams, H. Zaccone, W. Zeller and A. Zylberstejn.

1.- INTRODUCTION

The UA2 experiment (1), installed at the CERN $p\bar{p}$ collider (2), took the first data at the end of the 1981.
The main goal of the experiment is to detect the weak intermediate bosons Z^0 and $W^{\pm}$ in their electronic decay modes:

$$p\bar{p} \rightarrow Z^0 + X^0 \qquad Z^0 \rightarrow e^+ + e^-$$

$$p\bar{p} \rightarrow W^{\pm} + X^{\mp} \qquad W^{\pm} \rightarrow e^{\pm} + \nu(\bar{\nu})$$

For this reason electron identification is instrumented over 80% of the total solid angle by lead-scintillator sandwich counters, providing an acceptance of $\simeq$70%. Hadron detection is also instrumented in the central region by iron-scintillator sandwich counters in order to study high-p_T hadron jets.

Theory (3) predicts an electron-positron asymmetry in the W decay, with a significant signal between 20^o and 30^o. The UA2 forward-backward (F/B) spectrometers cover the polar angular regions from 20^o to 37.5^o and from 142.5^o to 160^o where a toroidal magnet is instrumented: together with a high accuracy vertex detector, the F/B drift chambers allow charge measurements on electrons up to 60 GeV/c momentum.

An azimuthal wedge of 30^o, opened in the central calorimeter, is equipped as a magnetic spectrometer wich is very useful to investigate phenomena of relatively high cross section such as inclusive charged and neutral particle production at relatively high p_T and new stable charged particles with or without fractional charge.

2. EXPERIMENTAL APPARATUS

An plan view of the UA2 detector is shown in Fig.1.

The measurement of the interaction point and of the particle trajectories in absence of magnetic field is achieved by means of the vertex detector which consists of four multiwire proportional chambers (MWPC) with helicoidal cathode strip read-out, two Jade-type drifts chambers with 24 cells each, for a total of 288 wires equipped with multihit read-out and charge division, 24 scintillation counters, arranged as a cylindrical hodoscope; a fifth MWPC, preceded by 1.5 radiation lenghts of tungsten , is used for shower localization in front of the electromagnetic central calorimeter. For the results presented here the informations from the vertex detector is used to separate $p\bar{p}$ events from background and to determine the collision point with a precision of $\pm$ 1 mm along the beam line.

The vertex detector is surronded by a central calorimeter with consists of lead-scintillator electromagnetic and iron-scintillator hadron counters covering polar angle θ from 40^{o} to 140^{o} and azimuthal angle ϕ from 30^{o} to 330^{o}. In the present stage of the experiment the remaining azimuthal angle ($\pm$ 15^{o} around the horizonthal plane) is covered by a single spectrometer which allow for the measurement of charged and neutral particle at 90^{o} degrees. A detailed description of the performances of the central calorimeter will be object of another report at this conference (4). The forward and backward regions (polar angle $20^{o} < \theta < 37.5^{o}$ and $142.5^{o} < \theta < 160^{o}$, respectively) are instrumented by 12 toroidal magnet sectors (B.l = .38 T.m) followed by 3x3 drift chamber planes for the charged tracks momentum measurement. In the

sector three trapezoidal chambers have 3 sensitive planes each with sense wire at -7^{o}, 0^{o}, $+7^{o}$ respect to the magnetic field direction: their space resolution of 250 μm will allow a $\Delta p/p = .006\ p$ that is adeguate to measure the particle charges for the determination of the $W^{\pm} \rightarrow e^{\pm}\nu(\bar{\nu})$ charge asymmetry.The drift chambers are then followed by a 1.4 radiation length thick iron-lead converter and four layers of multitube proportional chambers (MTPC) whose purpose is to localize electromagnetic showers. Electromagnetic calorimeter sectors finally complete the F/B detectors. Also the F/B calorimeters will be described in more detail in another report at this conference (4). Finally, the wedge detector (Fig. 2) is a single arm spectrometer covering 22^{o} in azimuth and 68^{o} in polar angle around $\theta = 90^{o}$. Two coils produce a field whose integral is 1.1 T.m and uses the calorimeter iron as return yoke. The spectrometer consists of 12 drift chambers planes, with wires at $+7^{o}$, 0^{o}, -7^{o} respect to the vertical direction, for the measurements of the charged particle trajectories. Combining the measurement of the interaction point coming from the vertex detector and the determination of the particle trajectories coming from the chambers, the charged particle momentum can be measured with a resolution of

$$\Delta p/p = \left((.5)^{2} + (.5p)^{2}\right)^{1/2} \qquad (p \text{ in GeV/c})$$

The chambers are then followed by a scintillator-iron-scintillator sandwich. Both scintillator hodoscope consists of 28 vertical counters. Each counter of the front hodoscope is equipped

with two PM's, for time-of-flight (TOF) measurements over a distance of 2.5 m with a resolution of .48 nsec. The counters after the 2 cm thick iron plate act as a preshower counters for the lead-glass wall wich completes the spectrometer. The lead-glass wall (Fig. 3) consists of 28 vertical columns of 10 cells, staggered as shown in Fig. 3 , each cell being a lead-glass block 14.5 radiation length deep, 15x15 cm^2 in cross section. At this stage of the experiment 2 columns of the lead-glass array have been replaced by a set of five scintillations counters for dE/dx measurements. The energy resolution of the lead glass wall has been measured to be

$$\sigma_E/E = (11.6 + 32.5/E)^{1/2} \ \% \qquad (E \text{ in GeV})$$

Each block has been calibrated using 10 GeV electrons, and is monitored with a Xe light flasher system; the calibration remained stable to within $\pm$ 2% during the $\bar{p}p$ running period.
The dE/dx counter mentioned above is used to search for fractionally charged particles (quarks) As shown in Fig. 4, it consists of 5 plexiglop plates 100 cm high, 30 cm wide and 4 cm thick; the light is collected at the top and bottom ends of each plate. Veto counters covering the light guides are used to reject events with particles crossing the light guides and faking a small ionization in the counters. This dE/dx counter has been calibrated at the CERN PS and its response to MIP has been studied as a function of the impact point.
Two scintillator arrays detecting small angle secondaries are used to discriminate against events from sources other than

beam beam collisions. Each array, covering one unit of rapidity around y = ± 4.7, is situated ± 10.3m away from the interaction point. All triggers require a coincidence of signals from the two hodoscopes,, wich are also used for the luminosity evaluation. The total integrated luminosity for which we present results is 75 μb^{-1}, calculated under the assumption that the non diffractive $\bar{p}p$ cross section at $\sqrt{s}$ = 540 GeV is 38 mb; the systematic error in the luminosity measurement has been estimated to be ± 17%.

3. INCLUSIVE π^o PRODUCTION[5]

The produced π^o's are identified from 2 photon decays, with the photons separately measured; the mean production angle is $\theta = 90^o$ and the π^o transverse momentum covers the range $1.5 < p_T < 4.5$ GeV/c.

The trigger for π^o detection required a coincidence between a signal from each of the two luminosity counters and a total energy deposition in the lead-glass wall exceeding a predefined threshold of 1.1 GeV. The energy deposition is reduced to a number of cluster defined as a set of adjacent cells with energy greater than 100 MeV; the minimum spatial separation of two resolved cluster is about 25 cm. Only events having at least 2 clusters of more than 200 MeV in the lead-glass wall are selected; if a track, as measured in the drift chambers, crosses the lead-glass wall at a distance less than 12 cm from the cluster center, the event is rejected since the cluster is attributed to a charged hadron, implying a loss of 2 ± 1% of real π^o decays.

The invariant mass distribution of the $\gamma\gamma$ sample is shown in Fig. 5 where a π^o peak is clearly visible over a combinatorial back-

ground of 20 to 30% depending on the transverse momentum.
From the Monte Carlo calculation (solid line in Fig. 5), a 4% readjustement of the energy scale was needed to get agreement with the data: this deviation could be attributed to the extrapolation of 10 GeV electron calibration of lead-glass to photons in the GeV range.
The acceptance is limited at low p_T by solid angle and a high p_T by the probability of both photons of merging into a single cluster: it is calculated from the Monte Carlo simulation and varies from .15 to .27 having a maximum at p_T = 2.7 GeV/c. The luminosity, measured from the left-right coincidences of the luminosity counters, has a 16% uncertainty coming from the reliability of these counters.
The p_T dependence of the invariant cross section for inclusive π^o production is shown in Fig. 6. The solid line of Fig. 6 shows the measured pion production in the $\sqrt{s}$ = 53 GeV pp collisions at ISR (6) in the p_T range of this experiment. At high transverse momentum we observe a large increase of the π^o cross section when the energy rises from 53 to 540 GeV.
In the inset of Fig. 6, an enhancement in the region of the η mass is clearly visible; this $\gamma\gamma\gamma$ mass distribution is obtained when more severe selection criteria are applied. An amount of 53 ± 15 events above background is observed: this is consistent with an estimate of 48 events obtained from a Monte Carlo calculation under the assumption that the inclusive cross section for η and π^o production are in the ratio .55 as measured in the ISR energy range (7).

The inclusive single photons production has been investigated comparing the transverse momentum distribution of a restricted photon sample with the prediction of a Monte Carlo simulation using as input the measured π^o cross section, and assuming a p_T independent η/π^o ratio equal to .55. In the p_T range between 1.5 and 3 GeV, a raw excess of 24 ± 58 photons has been observed. After corrections for a possible non linearity in the energy response of the lead glass and for a possible contamination on neutral hadrons, mostly antineutrons, a deficit of 46 ± 90 photons is obtained; a 95% confidence level upper limit is set for the single photons production $\gamma/\pi^o < 7.5\%$ in the p_T range between 1.5 and 3 GeV.

The technique used in the lead-glass array to measure π^o has also been applied to the forward-backward electromagnetic calorimeters. The inclusive cross-section obtained from these data covers a p_T range of .5 to 2.2 GeV/c and a rapidity between 1.1 and 1.7. The measurement (not shown) is in good agreement with the fit performed on the π^+,π^-,π^o cross section at 90^o (see section 4).

4. INCLUSIVE CHARGED PARTICLE PRODUCTION [8]

Charged particle production at 90^o has been investigated in the wedge detector.

The trigger required a beam-beam collision signed by the left-right coincidence of the luminosity counters and a coincidence of W_F and W_B hodoscope defining the presence of a charged track in the spectrometer. The matching of the track direction after bending,

as defined by the set of 12 drift chambers planes,and of the interaction point, as defined by the vertex detector, allows for the momentum and charge determination of a particle. In addition time-of-flight measurements in the W_F hodoscope provide the particle identification: K are separated from π up to momenta of 1.1 GeV/c and p from π and K up to 1.8 GeV/c.

The detector acceptance as a function of transverse momentum is computed using a Monte-Carlo program for the 3 particle types (π,K,p). Particles are generated with flat rapidity y and azimuthal angle ϕ distributions. The tracking of each particle through the spectrometer takes into account the detector geometry and field map, as well as multiple scattering and particle decay effects. Corrections have been applied for the loss of tracks due to nuclear interactions, which occur mainly in the vacuum pipe and in the vertex detector chamber walls. The wedge chambers efficiencies have been measured, resulting in a mean track reconstruction efficiency of 98%.

The quality and efficiency of the vertex finding in the vertex detector have been monitored using the tracks of the wedge or the F/B spectrometers in special runs where the magnetic fields were off. The vertex finding efficiency is at least 97%.

The integrated luminosity is 5 μb^{-1}; . a $\pm$ 17% systematic error reflects the run to run fluctuations(5).

The invariant cross section of inclusive hadron production (charge averaged) is displayed as function of p_T on Fig. 7a in the p_T range 0.4 to 2 GeV/c. The positive to negative ratio is measured to be 1.008 $\pm$ 0.021. It is p_T independent and consistent with unity as expected (Fig. 7b).

For each particle type, the positive to negative ratio is also p_T independent and consistent with 1, namely

$$\frac{\pi^+}{\pi^-} = 1.006 \pm 0.025, \quad \frac{K^+}{K^-} = 0.94 \pm 0.06, \quad \frac{p}{\bar{p}} = 1.01 \pm 0.09$$

The invariant cross sections for π, K, p, shown on Fig. 8a are therefore charge averaged.

The charged kaon production is in good agreement with a K_s measurement (9).

In Fig. 9, $\pi^{\pm}$ and π^o cross sections measured in this experiment (5) and at the ISR (10) are displayed. We observe a good agreement between our charged and neutral pion cross sections. Compared to ISR data, we note an increase of the pion cross section by a factor of 2 at 0.4 GeV/c, reaching a factor of 4 at 1.4 GeV/c. Charged and neutral pion data can be fitted to the empirical from:

$$E \frac{d^3\sigma}{dp^3} = A \left(\frac{2}{1+p_T}\right)^n$$

with A = 1.43 mb $GeV^{-2}c^3$, n = 8.3 ± 0.2 and p_t in GeV/c.

In contrast to the ISR results (11), the data cannot be fitted by an exponential law in the p_T range below 1 GeV/c.

Ratios of particle productions evaluated at the same transverse mass ($M_T = \sqrt{p_T^2 + M^2}$, where M is the particle mass) have been observed to be M_T independent at ISR energies. Fig. 8b gives the ratio K/π and p/π as function of M_T. No M_T dependence is found. Averaging over the measured range we get:

$$\frac{K}{\pi} = 0.39 \pm 0.02 \text{ (stat.)} \pm 0.03 \text{ (syst.)}$$

and

$$\frac{p}{\pi} = 1.02 \pm 0.05 \text{ (stat.)} \pm 0.05 \text{ (syst.)}$$

While the p/π ratio appears to be similar to the $\bar{p}/\pi^-$ ratio measured at the ISR, the K/π ratio has increased from ISR to SPS collider enrgies by 40%. This is possibly due to a more copious production of heavy flavors.

Charged particle production has been investigated also in the F/B sepctrometer starting from events selected with the minimum bias trigger wich requires a beam-beam collision signed by the left--right coincidence of the luminosity counters.

Using the same rechnique as in the wedge detector, but without particle identification, preliminary results based on meagre statistics have been obtained as far as the inclusive cross section is concerned: the charged particle p_T spectrum, ranging from .5 to 2.2 GeV/c, averaged on the rapidity interval from $\pm$ 1 to $\pm$ 1.8, is shown in Fig. 7a; the positive to negative ratio is consistent with 1 and p_T independent, as shown in Fig. 7b.

5. SEARCH FOR FRACTIONALLY CHARGED PARTICLES[12]

As mentioned before, in the data collected so far, the apparatus was such that two columns of the lead glass array have been replaced by a set of five scintillator counters Q_1 to Q_5 used for dE/dx measurements (Fig. 4). In this configuration a trigger sensitive to charged particles with fractional electric charge was constructed by linearly adding the amplified signals from the top and bottom phototubes of each counter Q_1 to Q_5 and

requiring that at least three out of the five signals so obtained exceed a threshold corresponding to an ionisation of 0.05, if we define as unity the most probable pulse height of minimum ionizing particles (MIPs). A further coincidence requirement was that both phototubes from either one of the two W_F counters in front of the Q-telescope give outputs above a threshold corresponding to an ionization of 0.03.

In order to suppress background from sources other than $\bar{p}p$ collisions, the trigger also required a coincidence with a minimum bias event.

During data taking the typical trigger rate was 0.02 s^{-1} at a luminosity of 10^{26} $cm^{-2}s^{-1}$. A total number of 15062 traiggers was recorded, corresponding to an integrated luminosity of 75 μb^{-1}.

In the data analysis, events are selected requiring 6 ionisation measurements from W_F and Q_1 to Q_5 counters corrected for the possible impact point position; then the most probable ionization I_o has been estimated by means of the likelyhood method allowing for the rejection of events inconsistent with a single I_o value. Events with signals from veto counters are also rejected. Further selection criteria have been applied to reject background events due to particles passing nearby the dE/dx counters or traversing it only partially. The I_o distribution of the remaining events is shown in Fig. 10a; there are 23 events, shown in Fig. 10b, which have abnormally low ionization, $I_o < .7$. A careful examination of these events shows that 15 of them can be explained as interactions in the iron plate or in the last two counters Q_4 and Q_5; the remaining 8 events are shown as shaded area in the distribution of Fig. 10b.

The requirement that, for events with $I_o > .5$, at least 6 out of 12 drift chamber planes have a hit in front of the Q counters and the additional request that no energy deposition be present in either of the two columns of lead glass counters adjacent to the Q-telescope, leaves no events in the sample of events with $I_o < .7$.

This null result can be expressed as an upper limit for the ratio R_Q of the quark yield around 90^o to that of particles with unit electric charge. The 90% conficence level upper limit is given by the relation

$$2.3 = N_{MB}\ \alpha_Q\ R_Q$$

where α_Q is the detection efficienty and N_{MB} is the total number of minimum bias events recorded during the experiment.

The detection efficiency is calculated using a Monte-Carlo simulation program. It depend on the geometry of the detector, on the quark mass and momentum spectrum because of the detector thickness of $\sim$ 40 gr cm^{-2} between the $\bar{p}p$ collision point and counter Q_5, and on the deflection of the particle trajectories due to the magnetic field of the spectrometer. Quarks of various masses m_Q and electric charge equal to $\pm$ 1/3 and $\pm$ 2/3 are generated in the Monte Carlo simulation with a flat rapidity distribution around 90^o, and with a transverse momentum distribution of the form $p_T \exp(-Bm_T)$, where $m_T = (p_T^2 + m_Q^2)^{\frac{1}{2}}$ and $B = 5\ (GeV/c^2)^{-1}$ as suggested by thermodynamical models for particle production (13). The behaviour of α_Q is reflected in Fig. 11, which shows the 90% confidence level upper limit for the ratio R_Q as a function of the quark mass m_Q, for both 1/3 and 2/3 quark charges.

In conclusion, no evidence for particles with fractional electric charge has been found at the CERN $\bar{p}p$ collider ($\sqrt{s}$ = 540 GeV). The yield of light quarks with charge 1/3 or 2/3 is at most 1/5000 of that of particles with unit charge. The sensitivity of the measurement decreases with increasing quark masses and at m_Q = 2 GeV/c^2 the upper limit of the ratio of quark yield to that of particles with unit charge becomes 2.5×10^{-3} for quarks with charge 2/3 and 10^{-3} for quarks with charge 1/3.

6. CONCLUSIONS

The inclusive π^o production from $p\bar{p}$ collisions at $\sqrt{s}$ = 540 GeV has been measured in the p_T range 1.5 to 4.5 GeV/c: it is larger than that measured in pp collisions at ISR energy. An η signal has been measured, consistent with η/π^o = .55 as measured at the ISR. No evidence has been found for photon sources other than π^o and η production.

The inclusive charged hadron production has also been measured with particle identification below 1.4 GeV/c for protons and 1.1 GeV/c for kaons: in this range the particle ratios are transverse mass idenpendent and, while the $\bar{p}/\pi$ ratio shows little change compared to the ISR, the K/π ratio has increased by 40%.

Charged and neutral pion inclusive cross section can be fitted to the empirical form:

$$E\, d^3/dp^3 = A \left(\frac{2}{1+p_T}\right)^n$$

with A = 1.43 mb GeV$^{-2}c^3$, n = 8.3 $\pm$0.2 and p_T in GeV/c.

Concerning the search for relativistic particles with fractional electric charge, no evidence has been found for such particles:

the yield of light quarks with charge 1/3 or 2/3 is at most 1/5000 of that of particles with unit charge.

ACKNOWLEDGEMENTS

We deeply acknowledge the help of the technical staffs of the Institutes Collaborating in UA2.
The author would also like to thank the organisers for an enjoyable conference. I also thank Mrs. R.Marchini and A.Montagna for their help in producing a written version of this talk.

REFERENCES

1) UA2 Collaboration, M. Banner et al., CERN/SPS/78-08 (1978) and CERN/SPS/78-54 (1978);
UA2 Collaboration, M. Banner et al., contribution to the International Conference on Experimentation at LEP, Uppsala, 15-20 June 1980.
UA2 Collaboration, M. Banner et al., First results from the UA2 experiment at the SPS $p\bar{p}$ collider, Proceedings of the V Warsaw Symposium on Elementary Particle Physics, Kazimierz, Poland, 24-28 May 1982, pg. 7.
2) The Staff of the CERN proton-antiproton project, Phys. Lett. 107B (1981) 306.
3) See, for example:
C. Quigg, Rev. Mod. Phys. 44 (1977) 297.
4) UA2 Collaboration, Invited talk presented by P. Darriulat at this Conference.
5) M. Banner et al., Phys. Lett. 115B (1982) 59.
6) B. Alper et al., Nucl. Phys. B87 (1975) 19 and Nucl. Phys. B100 (1975) 237.
K. Eggert et al., Nucl. Phys. B98 (1975) 49.
F.W. Büsser et al., Nucl. Phys. B106 (1976) 1.
A.G. Clark et al., Nucl. Phys. B142 (1978) 189.
7) F.W. Büsser et al., Phys. Lett. 55B (1975) 232.
K. Eggert et al., Nucl. Phys. B98 (1975) 49.
C. Kourkoumelis et al., Phys. Lett. 84B (1979) 277.
8) UA2 Collaboration, M. Banner et al., Inclusive Charged Particle Production at the CERN $\bar{p}p$ Collider (to be published in Physics Letters).
9) K. Alpgard et al., Phys. Lett. 115B (1982) 65.
10) M. Banner et al., Phys. Lett. 41B (1972) 547.
B. Alper et al., Nucl. Phys. B87 (1975) 19 and Nucl. Phys. B100 (1975) 237.
11) T. Akesson et al., Phys. Lett. 108B (1982) 58.

12) UA2 Collaboration, M. Banner et al., A Search for Relativistic Particles with Fractional Electric Charge at the CERN $p\bar{p}$ collider (to be published in Physics Letters).

13) R. Hagedorn and J. Ranft, Suppl. Nuovo Cim. 6 (1968) 169; R. Hagedorn, Suppl. Nuovo Cim. 6 (1968) 311.

FIGURE CAPTIONS

Fig. 1: Plan view of the UA2 detector.

Fig. 2: Side view of central part of the UA2 detector showing the single arm large angle spectrometer (wedge detector).

Fig. 3: Exploded view of the wedge detector.

Fig. 4: Side (a) and top (b) view of the dE/dx counter implemented in the wedge detector.

Fig. 5: Invariant mass distribution of the two-photons sample (full dots). The distribution in the insert around the η mass is for stricter cuts (see text). The result of the Monte Carlo simulation (solid lines) has been added to a hand-drawn background (dashed lines).

Fig. 6: The measured invariant cross-section for $p\bar{p} \to \pi^0 + \ldots$ (full dots) at $\sqrt{s} = 540$ GeV is compared to that for $pp \to \pi^0 + \ldots$ at $\sqrt{s} = 53$ GeV (solid line). The pp data are from Ref. (6); in the lower P_T range the mean of π^+ and π^- cross-sections has been used. The dashed line is an extrapolation of the data of Ref. (6) to Collider energy using the form $p_T^{-8} (1-x_T)^9$.

Fig. 7: a) Invariant cross section for hadron production (charge averaged) (h = π+K+p).
b) Positive to negative ratio as function of p_t.

Fig. 8: a) Invariant cross section for π (triangles), K (full dots) and p (squares) production (charge average) as function of p_t.
b) The ratios K/π (crosses) and p/π (open circles) evaluated at the same transverse mass (M_t) as function of M_t.

Fig. 9: Invariant cross section for π (triangles) and π^0 (Ref. 5) (squares) measured in this experiment compared to ISR data from Alper et al. (see Ref. 10).
The solid line is the fit to our data (see text).

Fig. 10: a) Distribution of the most probable ionisation I_o.
b) Expanded view of the I_o distribution in the region of abnormally low ionisation. The shaded area represents the distribution for the eight events which cannot be explained as interactions in the iron plate or in the last two planes of the Q-telescope.

Fig. 11: The 90% confidence level upper limit for the ratio R_Q defined as the ratio of quark yield to the yield of particles with unit electric charge, as a function of the quark mass m_Q. The curves labelled 2/3 and 1/3 refer to the absolute values of the quark charges, respectively.

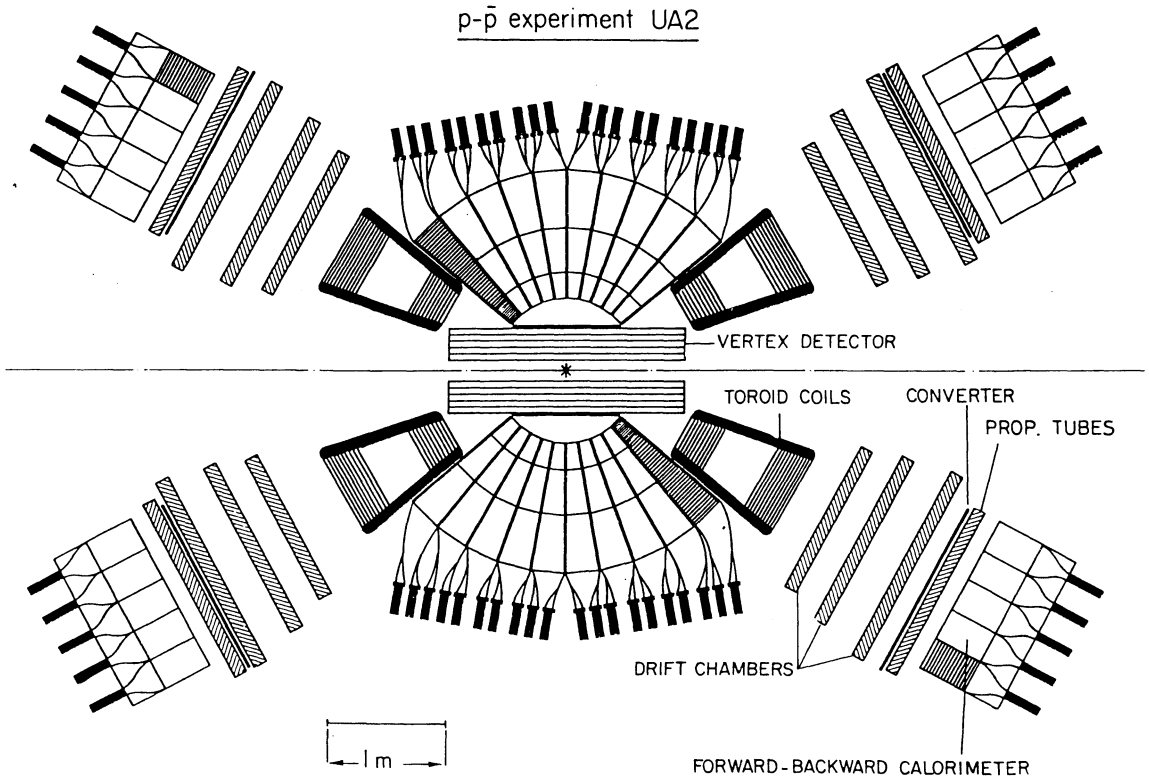
p-p̄ experiment UA2
VERTEX DETECTOR
TOROID COILS
CONVERTER
PROP. TUBES
DRIFT CHAMBERS
1 m
FORWARD-BACKWARD CALORIMETER

Fig. 1

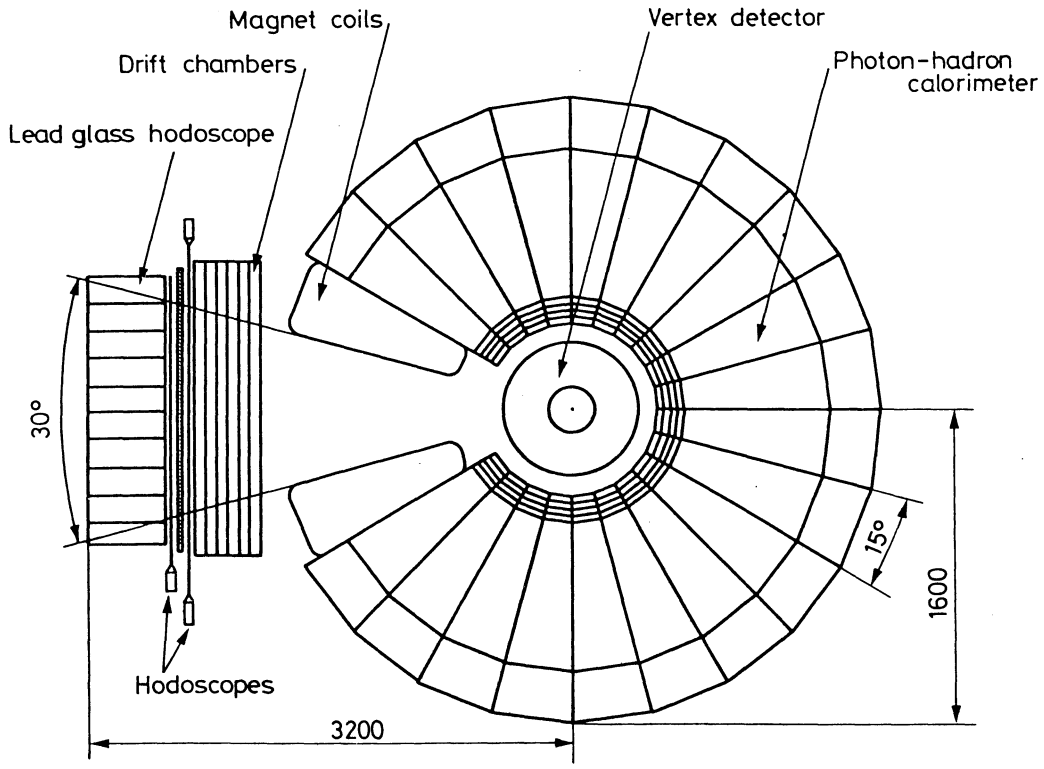
Magnet coils
Vertex detector
Drift chambers
Photon-hadron calorimeter
Lead glass hodoscope
30°
15°
1600
Hodoscopes
3200

Fig. 2

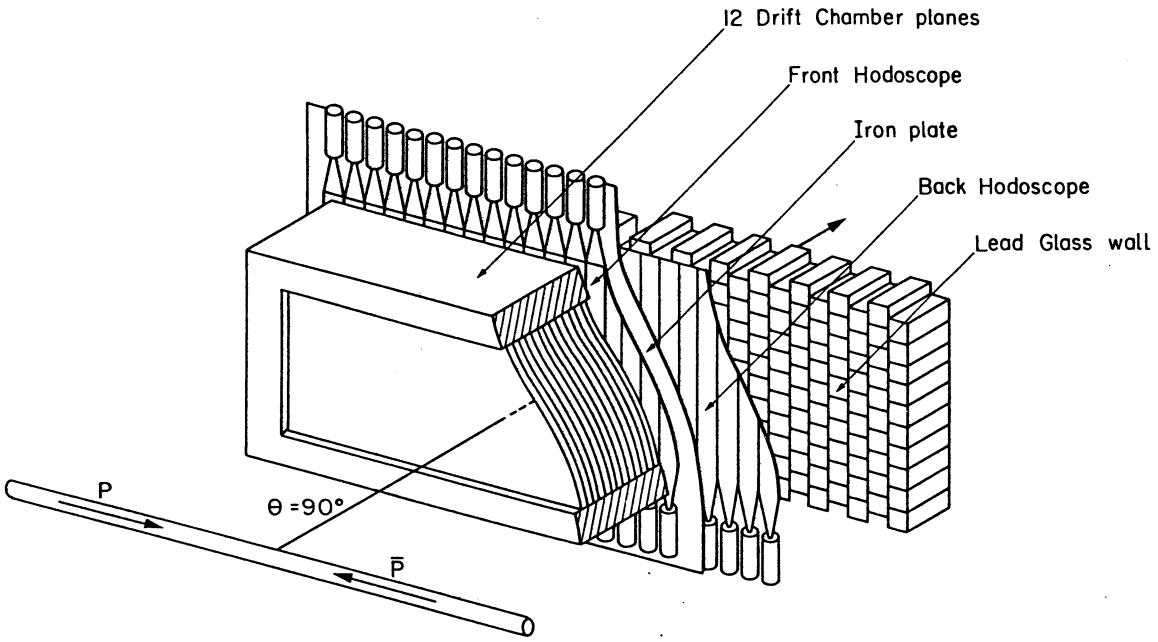
12 Drift Chamber planes
Front Hodoscope
Iron plate
Back Hodoscope
Lead Glass wall
P
θ =90°
P̄

Fig. 3

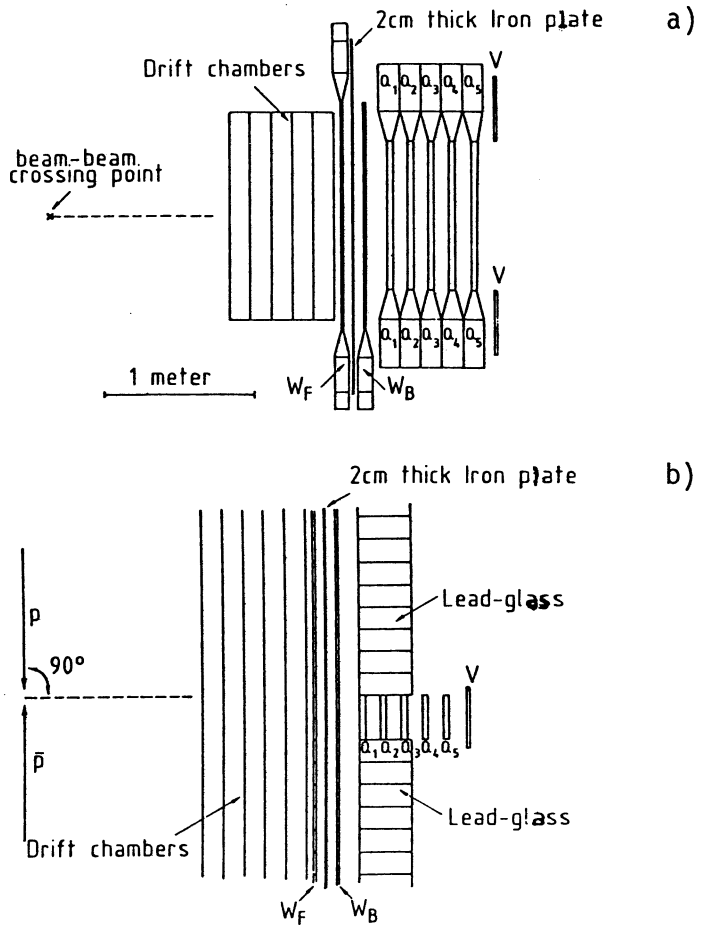
2cm thick Iron plate
a)
Drift chambers
V
beam-beam crossing point
1 meter
W_F
W_B
2cm thick Iron plate
b)
p
90°
p̄
Lead-glass
Drift chambers

Fig. 4

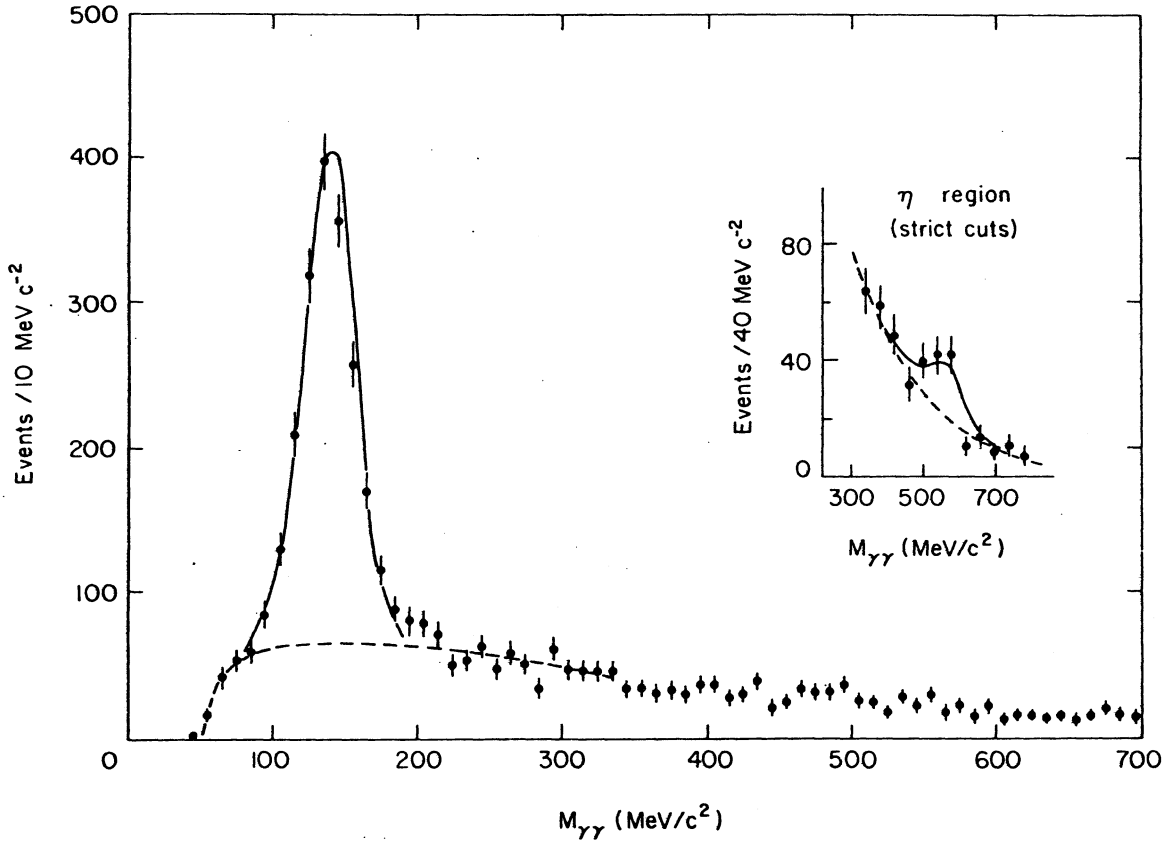
Events /10 MeV c^{-2}
$M_{\gamma\gamma}$ (MeV/c^2)
η region
(strict cuts)
Events /40 MeV c^{-2}
$M_{\gamma\gamma}$ (MeV/c^2)

Fig. 5

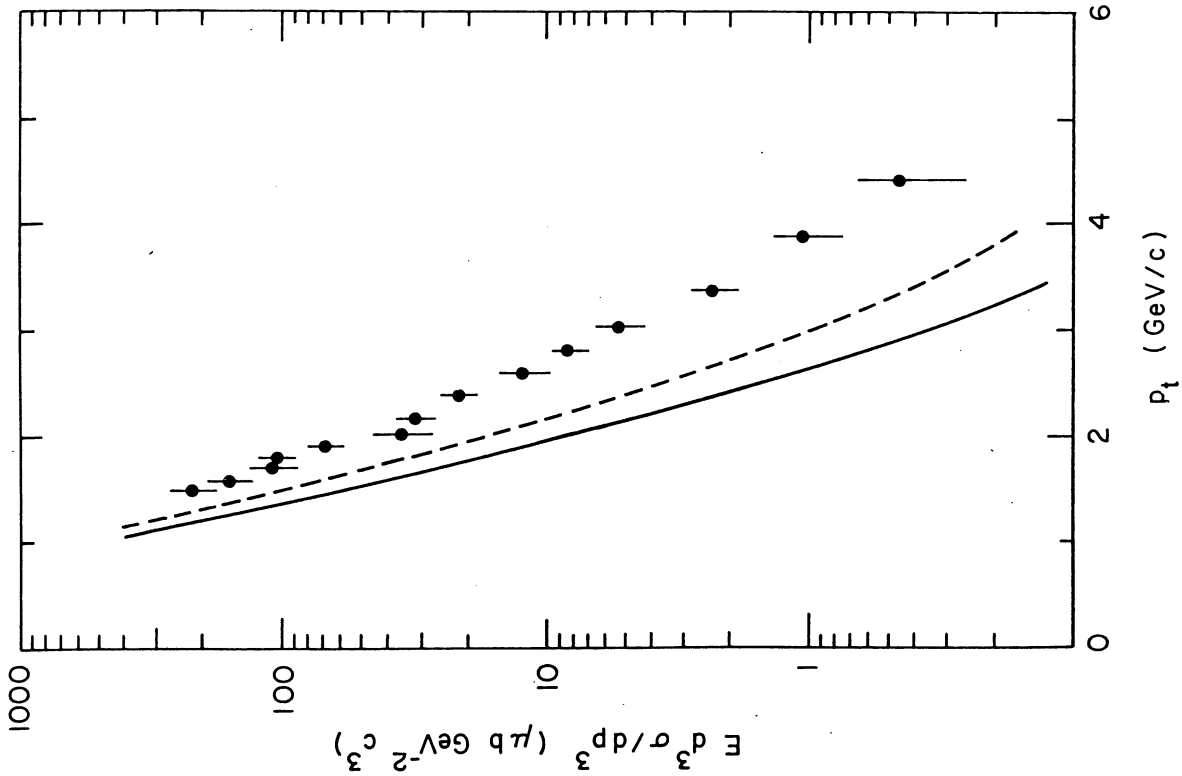
E d³σ/dp³ (μb GeV⁻² c³)
1000
100
10
1
0
2
4
6
p_t (GeV/c)

Fig. 6

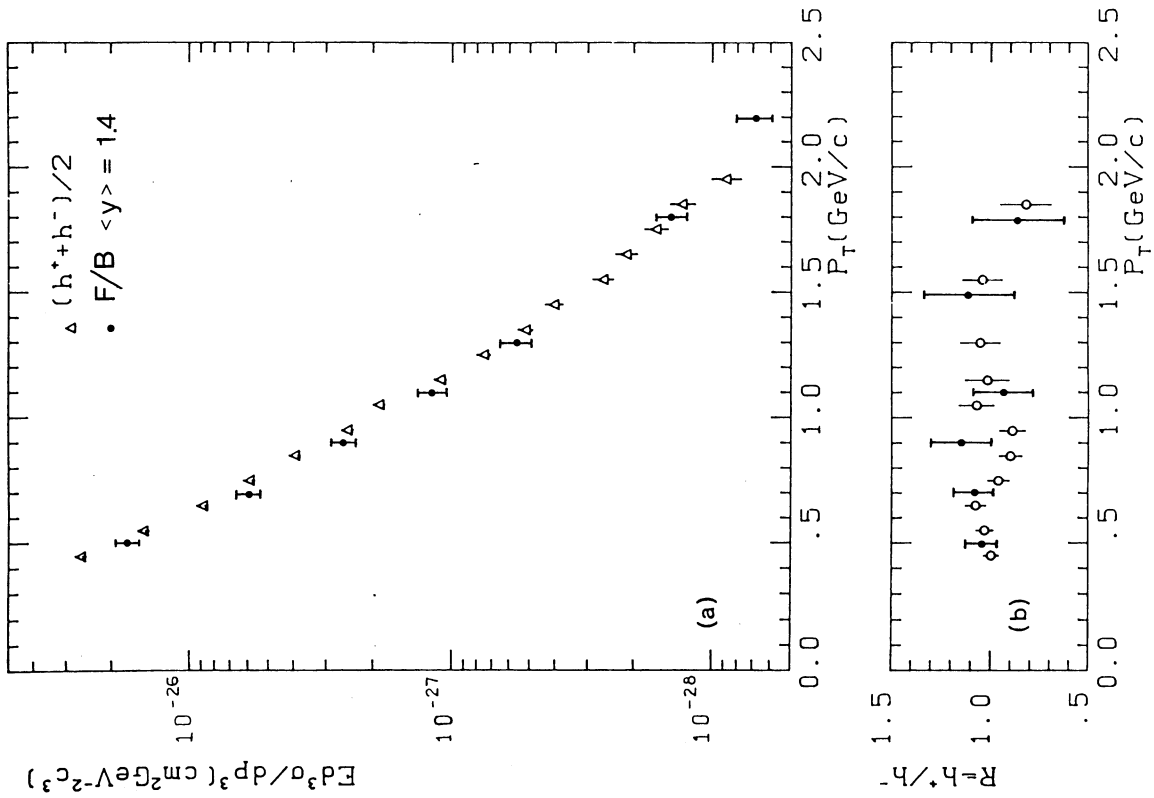
Ed³σ/dp³(cm²GeV⁻²c³)
10⁻²⁶
10⁻²⁷
10⁻²⁸
(h⁺+h⁻)/2
F/B <y> = 1.4
(a)
0.0
.5
1.0
1.5
2.0
2.5
P_T(GeV/c)
R=h⁺/h⁻
1.5
1.0
.5
(b)
0.0
.5
1.0
1.5
2.0
2.5
P_T(GeV/c)

Fig. 7

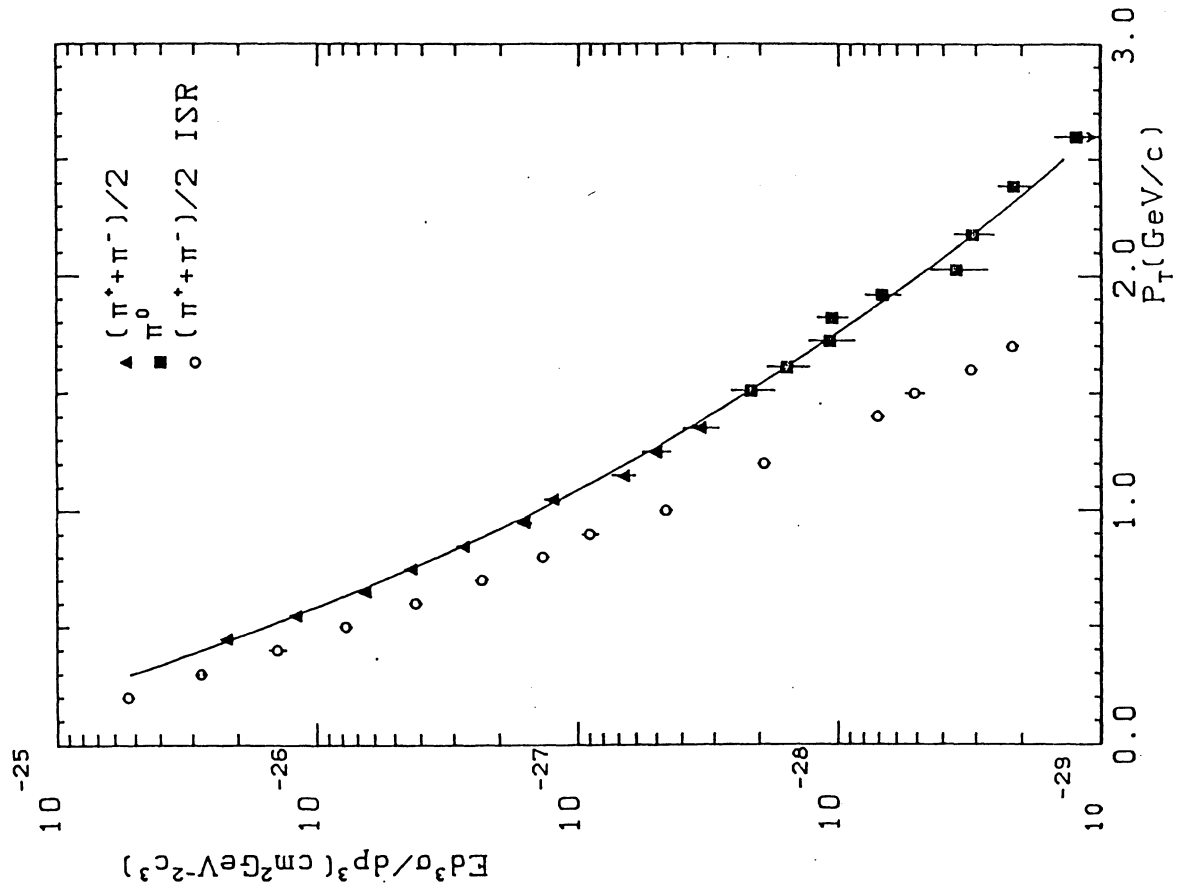
$Ed^3\sigma/dp^3$($cm^2GeV^{-2}c^3$)
$(\pi^+ + \pi^-)/2$
π^0
$(\pi^+ + \pi^-)/2$ ISR
P_T(GeV/c)

Fig. 9

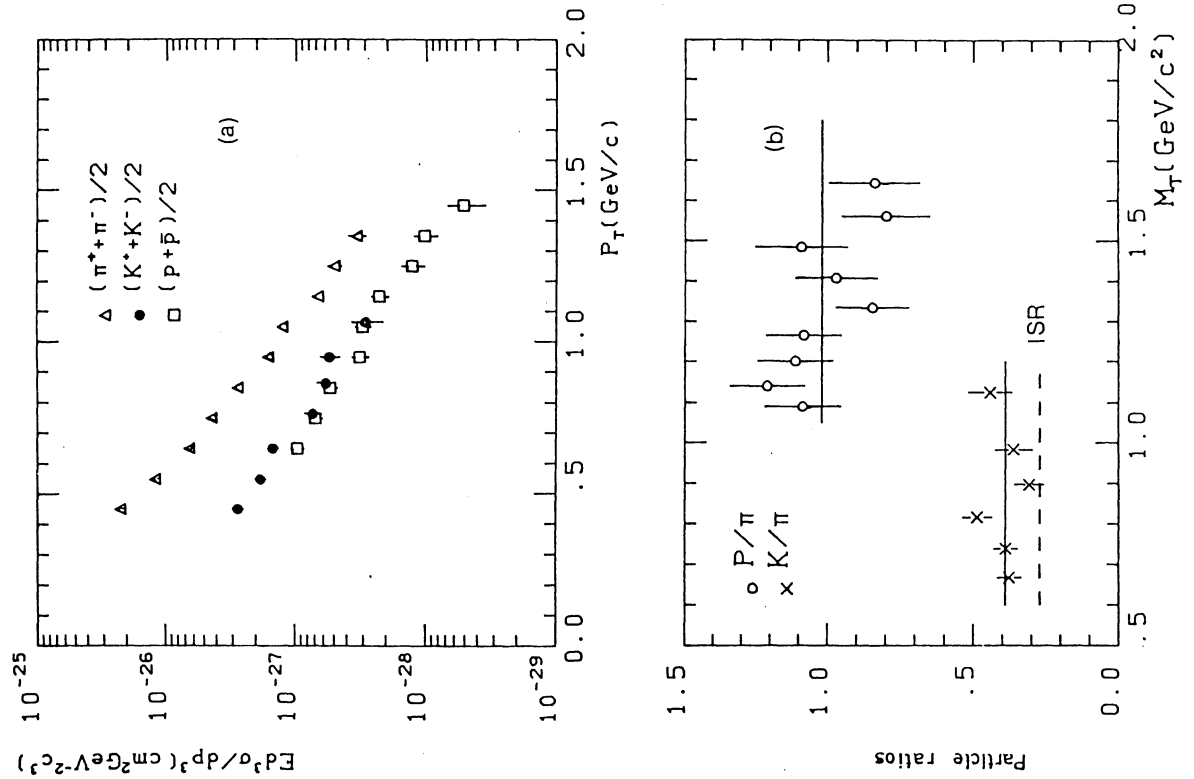
$Ed^3\sigma/dp^3$($cm^2GeV^{-2}c^3$)
(a)
$(\pi^+ + \pi^-)/2$
$(K^+ + K^-)/2$
$(p + \bar{p})/2$
P_T(GeV/c)
Particle ratios
(b)
P/π
K/π
ISR
M_T(GeV/c^2)

Fig. 8

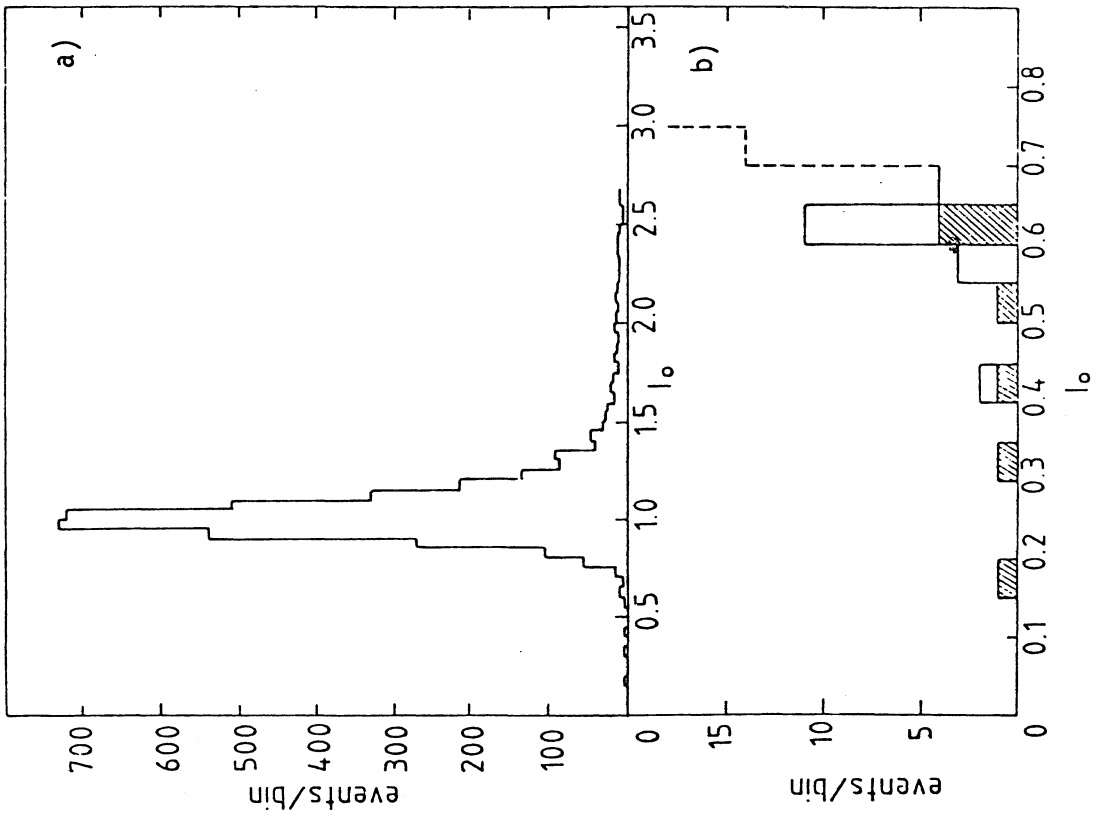
a)
b)
events/bin
I_o
0.1
0.2
0.3
0.4
0.5
0.6
0.7
0.8
0.5
1.0
1.5
2.0
2.5
3.0
3.5
100
200
300
400
500
600
700
0
5
10
15

Fig. 10

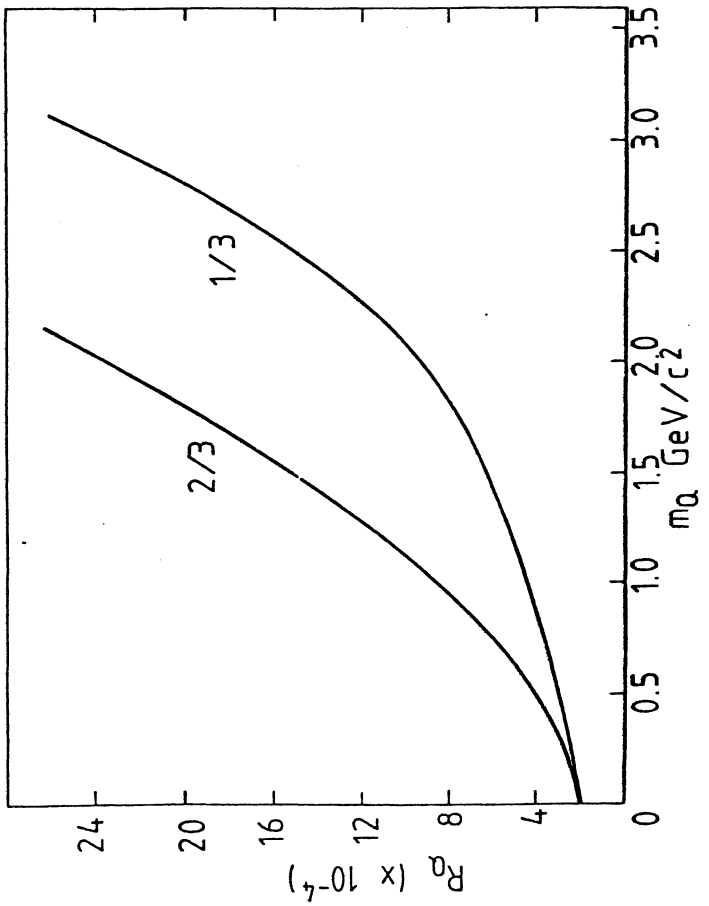
R_Q (x 10^{-4})
m_Q GeV/c^2
2/3
1/3
0
0.5
1.0
1.5
2.0
2.5
3.0
3.5
4
8
12
16
20
24

Fig. 11